APPLICATION OF TWO-STEP SPECTRAL PRECON-DITIONING TECHNIQUE FOR ELECTROMAGNETIC SCATTERING IN A HALF SPACE

D. Z. Ding, R. S. Chen, and Z. H. Fan [†]

Department of Communication Engineering
Nanjing University of Science and Technology
Nanjing 210094, China

Abstract—To efficiently solve large dense complex linear system arising from electric field integral equations (EFIE) formulation of half-space electromagnetic scattering problems, the multilevel fast multipole algorithm (MLFMA) is used to accelerate the matrix-vector product operations. The two-step spectral preconditioning is developed for the generalized minimal residual iterative method (GMRES). The two-step spectral preconditioner is constructed by combining the spectral preconditioner and sparse approximate inverse (SAI) preconditioner to speed up the convergence rate of iterative methods. Numerical experiments for scattering from conducting objects above or embedded in a lossy half-space are given to demonstrate the efficiency of the proposed method.

1. INTRODUCTION

There is significant interest in scattering from electrically large targets situated in the presence of a lossy half-space [1–4]. One of the principal tools for the analysis of such scattering is the method of moments (MoM) [5]. The electromagnetic integral equation is first discretized into a matrix equation using the Galerkin-based MoM with subdomain basis functions such as Rao-Wilton-Glisson (RWG) functions [6] for triangular patches. The formulation considered in this paper is the electric field integral equation (EFIE) as it is the most general and does not require any assumption about the geometry of the object. When iterative solvers are used to solve the MoM matrix equation, the

---

Corresponding author: D. Z. Ding (dzding@mail.njust.edu.cn).
[†] D. Z. Ding is also with Key State Key Laboratory of Millimeter Waves, Southeast University, China.

fast multipole algorithm (FMA) or multilevel fast multipole algorithm (MLFMA) [7] can be used to accelerate the calculation of matrix-vector products. The half-space MLFMA differs from the free-space MLFMA. In half-space MLFMA, the near interaction terms are evaluated efficiently via the complex-image technique [8, 9]. The far interaction terms are evaluated efficiently by employing the asymptotic form of the dyadic Green's function. Each component of the approximate Green's function is expressed in terms of the direct-radiation term plus radiation from an image source in real space [10]. The former accounts for the radiation of currents into the medium in which it resides, while the latter accounts for interactions with the half-space interface. The half-space MLFMA remains the same computational complexity of $O(N \log N)$ both in RAM and computational requirement (per iteration) as free-space MLFMA [1].

The system matrix resulted from EFIE with half-space MLFMA is often an ill-conditioned matrix and results in the low convergence of the Krylov iterative method [11]. Simple preconditioners like the diagonal or diagonal blocks of the coefficient matrix can be effective only when the matrix has some degree of diagonal dominance [12]. Incomplete LU (ILU) preconditioners have been successfully used on nonsysmmetric dense systems in [13], but the factors of the ILU preconditioner may become very ill-conditioned, and consequently the performance is very poor [14]. An effective sparse approximate inverse (SAI) preconditioner suitable for implementation in the FMM context has also been proposed [15], which is based on a Frobenius-norm minimization with a priori sparsity pattern selection strategy. Malas and Gurel proposed an efficient parallel SAI preconditioner combined with MLFMA in [16]. Andriulli et al. proposed a multiplicative calderon preconditioner for EFIE [17]. It has been shown that the MoM EFIE system obtained using the multiplicative calderon preconditioning converges rapidly, independent of the discretization density and that this technique outperforms more classical approaches like ILU or other general-purpose approximate inverses [18]. The performance of SAI preconditioner is greatly influenced by the way of choosing nonzero pattern and solving the least-squares problems in the minimization process. Information from free-space MLFMA implementation is employed to develop a high quality SAI preconditioner, resulting in a faster convergence rate [19]. Although the SAI preconditioner can improve matrix conditions by clustering most of the large eigenvalues close to one but still leave a few close to the origin, which can potentially slow down the convergence of Krylov methods. The presence of the smallest eigenvalues after preconditioning lies in that the construction of preconditioners is inherently local. Each degree

of freedom in the preconditioning matrix is coupled to only a few neighbors, and this compact support does not allow an exchange of global information. Inspired by the two-step preconditioning idea [20–22], the two-step spectral preconditioner is investigated to further enhance the quality of this SAI preconditioner, resulting in a faster convergence rate. In this method, the SAI preconditioner is used to damp the high frequencies of the error, while the spectral preconditioner in a two-level manner is applied to smooth the low frequencies of the error.

This paper is outlined as follows. Section 2 gives an introduction of half-space MLFMA theory. Section 3 describes the details to construct two-step spectral preconditioner. Numerical examples are given to demonstrate the accuracy and efficiency of the proposed method in radar cross section (RCS) calculations in Section 4. Section 5 gives some conclusions.

2. HALF-SPACE MLFMA THEORY

For solving the problem of scattering from an arbitrarily shaped perfectly electrically conducting (PEC) target situated above (i.e., tangent in layer $i = 1$) or buried ($i = 2$) in a lossy half space shown in Figure 1, we utilize the electric field integral equation (EFIE) [1]:

$$
\begin{aligned}
\widehat{\mathbf{n}} \times \mathbf{E}^{\mathrm{inc}}\left(\mathbf{r}\right) &= \widehat{\mathbf{n}} \times j\omega\mu_i \iint_{S'} \left[\overleftrightarrow{\mathbf{I}} + \frac{\nabla\nabla}{k_i^2} \right] \cdot \overleftrightarrow{\mathbf{G}}_{Aii}\left(\mathbf{r}, \mathbf{r}'\right) \cdot \mathbf{J}\left(\mathbf{r}'\right) dS' \\
&= \widehat{\mathbf{n}} \times \left[j\omega\mu_i \iint_{S'} \overleftrightarrow{\mathbf{K}}_{Aii}\left(\mathbf{r}, \mathbf{r}'\right) \cdot \mathbf{J}\left(\mathbf{r}'\right) dS' \right. \\
&\qquad \left. - \frac{\nabla}{j\omega\varepsilon_i} \iint_{S'} K_{\phi e}^{ii}\left(\mathbf{r}, \mathbf{r}'\right) \nabla' \cdot \mathbf{J}\left(\mathbf{r}'\right) dS' \right]
\end{aligned}
\tag{1}
$$

$\mathbf{E}^{\mathrm{inc}}$ and $\mathbf{J}(\mathbf{r}')$ denotes an incident field and the unknown surface current density, respectively. The unit vector $\widehat{n}$ is perpendicular to the scatterer surface. $\mathbf{r}$ and $\mathbf{r}'$ are the observation and source point, respectively. $\varepsilon_i = \varepsilon_i' - j\sigma_i/\omega$, μ_i and k_i represent (in general complex) the permittivity, permeability, and wavenumber of the medium in which the target resides, and ω is the angular frequency (an $e^{-i\omega t}$ time convention has been assumed and suppressed). Details on the dyadic Green's function $\overleftrightarrow{\mathbf{G}}_{Aii}$ and $\overleftrightarrow{\mathbf{K}}_{Aii}$ and on the scalar Green's function $K_{\phi e}^{ii}$ can be found in [23]. As in the MoM solution, the unknown surface
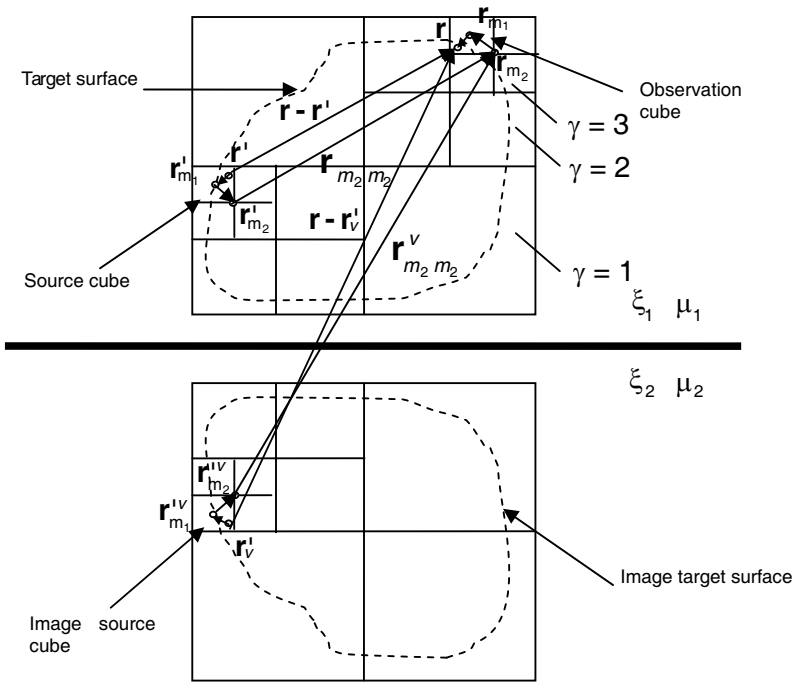
Figure 1. Geometry for source and observation group in 3-D MLFMA
and generalization to a half-space environment using real images to
account for far interface interactions.

current $\mathbf{J}$ is expanded into a set of N basis functions $\mathbf{b}_{n'}(\mathbf{r}')$

$$\mathbf{J}(\mathbf{r}') = \sum_{n'=1}^{N} I_{n'}\mathbf{b}_{n'}(\mathbf{r}') \tag{2}$$

where the RWG basis is used [6]. $I_{n'}$ is the unknown expansion
coefficients. Applying Galerkin's method results in a matrix equation

$$\mathbf{Z} \cdot \mathbf{I} = \mathbf{V} \tag{3}$$

The elements of the impedance matrix $\mathbf{Z}$ and the right side vector $\mathbf{V}$
are given by

$$\mathbf{Z}_{nn'} = j\omega\mu_i \iiint\limits_{S}\iiint\limits_{S'} \mathbf{b}_n(\mathbf{r}) \cdot \left[\overset{\leftrightarrow}{\mathbf{I}} + \frac{\nabla\nabla}{k_i^2}\right] \cdot \overset{\leftrightarrow}{\mathbf{G}}_{Aii}(\mathbf{r},\mathbf{r}') \cdot \mathbf{b}_{n'}(\mathbf{r}')\, dS'dS \tag{4}$$

$$V_n = \iint\limits_{S} \mathbf{b}_n(\mathbf{r}) \cdot \mathbf{E}^{\mathrm{inc}}(\mathbf{r}) dS \tag{5}$$

In the FMM or MLFMA implementation [7], the computation of interactions is divided into near $\mathbf{Z}^{\mathrm{near}}$ and far terms $\mathbf{Z}^{\mathrm{far}}$:

$$\mathbf{Z} = \mathbf{Z}^{\mathrm{near}} + \mathbf{Z}^{\mathrm{far}} \tag{6}$$

For near interactions $\mathbf{Z}^{\mathrm{near}}$, the evaluation of the impedance matrix elements remains the same as in MoM procedure. The dyadic half-space Green's function is evaluated using the discrete complex images method (DCIM) to avoid the direct numerical computation of sommerfeld integrals (SI). For far interactions $\mathbf{Z}^{\mathrm{far}}$, the half-space dyadic Green's function can be split into a "direct" contribution $\overleftrightarrow{\mathbf{I}} g_i$ between source and observation point and a remaining dyadic $\Delta\overleftrightarrow{\mathbf{G}}_{Aii}$ accounting for the interface (Δ is not an operator).

$$\overleftrightarrow{\mathbf{G}}_{Aii}(\mathbf{r},\mathbf{r}') = \overleftrightarrow{\mathbf{I}} g_i(\mathbf{r},\mathbf{r}') + \Delta\overleftrightarrow{\mathbf{G}}_{Aii}(\mathbf{r},\mathbf{r}') = \overleftrightarrow{\mathbf{I}} \frac{e^{-jk_i|\mathbf{r}-\mathbf{r}'|}}{4\pi\,|\mathbf{r}-\mathbf{r}'|} + \Delta\overleftrightarrow{\mathbf{G}}_{Aii}(\mathbf{r},\mathbf{r}') \tag{7}$$

Therefore, the matrix elements accounting for "far" interactions are also split:

$$\mathbf{Z}_{nn'}^{\mathrm{far}} = \mathbf{Z}_{nn'}^{\mathrm{far,hom}} + \Delta\mathbf{Z}_{nn'}^{\mathrm{far}} \tag{8}$$

$$\mathbf{Z}_{nn'}^{\mathrm{far,hom}} = j\omega\mu_i \iint\limits_{S}\iint\limits_{S'} \mathbf{b}_n(\mathbf{r}) \cdot \left[\overleftrightarrow{\mathbf{I}} + \frac{\nabla\nabla}{k_i^2}\right]$$
$$\cdot \mathbf{g}_i(\mathbf{r},\mathbf{r}') \cdot \mathbf{b}_{n'}(\mathbf{r}')\, dS' dS \tag{9}$$

$$\Delta\mathbf{Z}_{nn'}^{\mathrm{far}} = j\omega\mu_i \iint\limits_{S}\iint\limits_{S'} \mathbf{b}_n(\mathbf{r}) \cdot \left[\overleftrightarrow{\mathbf{I}} + \frac{\nabla\nabla}{k_i^2}\right]$$
$$\cdot \Delta\overleftrightarrow{\mathbf{G}}_{Aii}(\mathbf{r},\mathbf{r}') \cdot \mathbf{b}_{n'}(\mathbf{r}')\, dS' dS \tag{10}$$

The impedance matrix elements in free-space FMM or MLFMA accounting for "far" interactions are written as

$$\mathbf{Z}_{nn'}^{\mathrm{far,hom}} = \frac{\omega\mu_i k_i}{(4\pi)^2} \iint\limits_{4\pi} \mathbf{W}_{m\alpha}(\hat{\mathbf{k}}) \cdot T_L\!\left(k_i r_{m'm}, \hat{\mathbf{k}}\cdot\hat{\mathbf{r}}_{m'm}\right) \mathbf{B}_{m'\alpha'}\!\left(\hat{\mathbf{k}}\right) d^2\hat{\mathbf{k}} \tag{11}$$

$$\mathbf{W}_{m\alpha}\!\left(\hat{\mathbf{k}}\right) = \left[\overleftrightarrow{\mathbf{I}} - \hat{\mathbf{k}}\hat{\mathbf{k}}\right] \cdot \iint\limits_{S} \mathbf{b}_{n(m,\alpha)}(x)\, e^{-jk_i\hat{\mathbf{k}}\cdot(r-r_m)} dS \tag{12}$$

$$\mathbf{B}_{m'\alpha'}\left(\hat{\mathbf{k}}\right) = \left[\overset{\leftrightarrow}{\mathbf{I}} - \hat{\mathbf{k}}\hat{\mathbf{k}}\right] \cdot \iint_{S} \mathbf{b}_{n'(m',\alpha')}\left(\mathbf{x}'\right) e^{-jk_i\cdot\hat{\mathbf{k}}\cdot(r-r_m)}dS' \qquad (13)$$

$$T_L\left(k_i r_{m'm}, \hat{\mathbf{k}}\cdot\hat{\mathbf{r}}_{m'm}\right) = \sum_{l=0}^{L}(-j)^l(2l+1)h_l^{(2)}(k_i r_{m'm})P_l\left(\hat{\mathbf{k}}\cdot\hat{\mathbf{r}}_{m'm}\right) \ (14)$$

where (12) and (13) represent the plane-wave decomposition of basis and weighing functions, respectively. However, for a half-space MLFMA, it is essential to include the "far" interface interactions represented by $\Delta\mathbf{Z}_{nn'}^{\text{far}}$ in (10). In the complex-image technique, each component of the dyadic $\Delta\overset{\leftrightarrow}{\mathbf{G}}_{Aii}$ is expressed in terms of a sum of free-space Green's functions with image sources located in complex space [8, 9]. Therefore, the expansion (11) can be also applied to far interface interactions $\Delta\mathbf{Z}_{nn'}^{\text{far}}$. However, the number of terms L in (14) required for convergence can be prohibitively large for general complex source points, undermining the efficiency of using (11) for $\Delta\mathbf{Z}_{nn'}^{\text{far}}$ in the context of DCIM. Therefore, we use an approximate but highly accurate method for evaluating the far interface interactions. The FMA has been successfully extended to the scattering from a PEC object above or buried in a half space by employing the asymptotic form of the Green's function for far interactions [24]. The asymptotic form of the Green's function is represented utilizing a single real image at $\left[\hat{\mathbf{I}} - 2\hat{z}\hat{z}\right] \cdot r'$ (assuming the interface at $z = 0$). Because the image sources are located in real space, generalizing the free-space MLFMA to a half-space MLFMA is now straightforward. The translation operators between image cube and observation cube centers for all nonnearby cubes at all levels are written as

$$T_L\left(k_i r_{m'm}^v, \hat{\mathbf{k}}\cdot\hat{\mathbf{r}}_{m'm}^v\right) = \sum_{l=0}^{L}(-j)^l(2l+1)h_l^{(2)}(k_i r_{m'm}^v)P_l\left(\hat{\mathbf{k}}\cdot\hat{\mathbf{r}}_{m'm}^v\right) \ (15)$$

where $\hat{\mathbf{r}}_{m'm}^v$ is a vector from the image source group center to the observation group center in Figure 1. The Fourier transforms

$$\begin{aligned}\mathbf{B}_{m'\alpha'}^v\left(\hat{\mathbf{k}}\right) &= \left[\overset{\leftrightarrow}{\mathbf{I}} - \hat{\mathbf{k}}\hat{\mathbf{k}}\right] \cdot \left[\overset{\leftrightarrow}{\mathbf{I}} - 2\hat{z}\hat{z}\right] \cdot \iint_{S'} \mathbf{b}_{n'(m',\alpha')}\left(\mathbf{r}'\right) \\ &\quad \cdot e^{+jk_i\hat{\mathbf{k}}\cdot\left[\overset{\leftrightarrow}{\mathbf{I}}-2\hat{z}\hat{z}\right]\cdot(\mathbf{r}'-\mathbf{r}'_m)}dS'\end{aligned} \qquad (16)$$

of the image expansion functions $\left[\overset{\leftrightarrow}{\mathbf{I}} - 2\hat{z}\hat{z}\right] \cdot \mathbf{b}_{n'(m',\alpha')}\left(\mathbf{r}'\right)$, where $\overset{\leftrightarrow}{\mathbf{I}} - 2\hat{z}\hat{z}$ denotes the relative orientation and location of the image

expansion functions. Finally, the linear system of equations in (3) can be solved by the restarted GMRES iterative method [25] using MLFMA to accelerate the matrix-vector products.

3. TWO-STEP SPECTRAL PRECONDITIONER

The system matrix resulted from EFIE with half-space MLFMA is often an ill-conditioned matrix and results in the low convergence of the Krylov iterative method. MLFMA stores only the near-field matrix, which is composed of the strong electromagnetic coupling, resulting in matrix elements with relatively larger magnitudes. Furthermore, the near-field matrix in half-space MLFMA becomes sparser as the problem size increases [16]. Since the preconditioners are usually built based on near-field matrix, effective preconditioning becomes a challenge.

It is well known that the convergence rate of an iterative solution is dependent upon the spectral radius of the matrix equation system. In order to speed up the convergence rate of Krylov methods, preconditioning techniques are employed to transform the EFIE matrix equations into an equivalent form

$$\mathbf{M}_1 \mathbf{Z} \mathbf{I} = \mathbf{M}_1 \mathbf{V} \tag{17}$$

where $\mathbf{Z}$ is the EFIE impedance matrix associated with the higher order hierarchical basis functions, and $\mathbf{M}_1$ is the corresponding preconditioner. The purpose of preconditioning is to make the preconditioned matrix $\mathbf{M}_1 \mathbf{Z}$ better conditioned than the original matrix $\mathbf{Z}$. In the MLFMM context, the near-field matrix $\mathbf{Z}^{\text{near}}$ is widely used as the basis for constructing preconditioners. The preconditioner $\mathbf{M}_1$ is an improved sparse approximate inverse (MSAI) preconditioner based on $\tilde{\mathbf{Z}}^{\text{near}}$, where $\tilde{\mathbf{Z}}^{\text{near}}$ is the sparse form of $\mathbf{Z}^{\text{near}}$ [19].

Although the SAI preconditioner can improve matrix conditions by clustering most of the large eigenvalues close to one it leaves a few close to the origin, which can potentially slow down the convergence of Krylov methods. The presence of the smallest eigenvalues after preconditioning lies in that the construction of preconditioners is inherently local. Each degree of freedom in the preconditioning matrix $\mathbf{M}_1$ is coupled to only a few neighbors, and this compact support does not allow an exchange of global information. When the exact inverse of the original matrix is globally coupled, this lack of global information may have a severe impact on the quality of preconditioners. Although the discrete Green's function exhibits a rapid decay, the exact inverse of the impedance matrix is dense, thus has global support. The locality of preconditioners can be reduced by simply enlarging near-field matrix

$\mathbf{Z}^{\text{near}}$. However, the construction and implementation cost grows accordingly. Moreover, in the MLFMM context, the computation of additional entries from $\mathbf{Z}$ requires the approximation of surface integrals, where only entries of the near-field matrix $\mathbf{Z}^{\text{near}}$ are available.

In this case, some suitable mechanism has to be considered to recover global information. The spectral preconditioning technique in [20] can be used in a two-step way for the above SAI preconditioned system. The purpose here is to recover global information by removing the effect of some smallest eigenvalues in magnitude in the SAI preconditioned matrix, which can potentially slow down the convergence of Krylov solvers [26].

Let $\mathbf{U}_k$ be a set of eigenvectors of dimension k associated with the smallest eigenvalues of the MSAI preconditioned matrix $\mathbf{M}_1\mathbf{Z}$. The second level spectral preconditioner can then be defined as

$$\mathbf{M}_2 = \mathbf{I} + \mathbf{U}_k(\mathbf{T}_k^{-1} - \mathbf{I}_k)\mathbf{U}_k^H \qquad (18)$$

where $\mathbf{T}_k = \mathbf{U}_k(\mathbf{M}_1\mathbf{Z})(\mathbf{U}_k)^H$, and $\mathbf{I}$ and $\mathbf{I}_k$ are unit matrix of dimension N and k, respectively. The superscript H denotes the transpose and conjugate of a given complex matrix. Combining this second spectral preconditioner with the prescribed preconditoner in the two-level manner, a new two-step spectral preconditioner is derived, and the linear system to be solved can be transformed into

$$\mathbf{M}_2\mathbf{M}_1\mathbf{Z}\mathbf{x} = \mathbf{M}_2\mathbf{M}_1\mathbf{b} \qquad (19)$$

We consider two methods for computing an approximation to the eigenvectors that correspond to a few smallest eigenvalues. One way is to use the ARPACK software [27]. This is equal to solve another large eigenvalue problem with the same coefficient matrix of the problem at hand. This computation is very expensive. In this paper, the linear system is solved particularly with the SAI preconditioned GMRES-DR algorithm [28], which also generates approximations to eigenvectors as a byproduct. The approximate eigenvectors in GMRES-DR span a small Krylov subspace and so are generated in a compact form

$$(\mathbf{M}_1\mathbf{Z})\mathbf{V}_k = \mathbf{V}_{k+1}\bar{\mathbf{H}}_k \qquad (20)$$

where $\mathbf{V}_k$ is a $N \times k$ matrix, whose columns span the subspace of approximate eigenvectors; $\mathbf{V}_{k+1}$ is the same except an extra column; $\bar{\mathbf{H}}_k$ is a full $k+1$ by k matrix. Note that Equation (20) allows access to both the approximate eigenvectors and their products with SAI preconditioned matrix $\mathbf{M}_1\mathbf{Z}$ while requiring storage of only $k+1$ vectors of length N. Therefore, in order to construct the spectral preconditioner in a two-level manner, one can simply replace $\mathbf{U}_k$ with

$\mathbf{V}_k$ by appending zeros, $\mathbf{T}_{\underline{k}}$ with $\mathbf{H}_k$, where $\mathbf{H}_k$ is a full k by k matrix by discarding last row of $\mathbf{\bar{H}}_k$.

Therefore, a two-step spectral preconditioned GMRES algorithm is presented for solving systems of linear equations, as follows:

- Construct SAI preconditioning matrix $\mathbf{M}_1$.
- Solve the linear system with the SAI preconditioned GMRES-DR algorithm, and use generated eigenvector information to construct the spectral preconditioning matrix $\mathbf{M}_2$.
- Construct the two-level spectral preconditioning matrix $\mathbf{M} = \mathbf{M}_2\mathbf{M}_1$, and use it for GMRES algorithm to solve linear systems.

4. NUMERICAL EXPERIMENTS

In this section, we show some numerical results for open conducting structures in the presence of a half space that illustrate the effectiveness of the proposed two step spectral preconditioner for the solution of the EFIE linear systems. The EFIE linear systems based on the RWG basis functions are solved with MLFMM accelerated Krylov iterative methods. All numerical experiments are performed on a Pentium 4 with 2.9 GHz CPU and 2 GB RAM in single precision. The restarted version of GMRES (m) algorithm is used as iterative method, where m is the dimension size of Krylov subspace for GMRES. Additional details and comments on the implementation are given as follows:

- Zero vector is taken as initial approximate solution for all examples and all systems in each example.
- The iteration process is terminated when the normalized backward error is reduced by 10^{-3} for all the examples. The maximum number of iterations is limited to be 1000.
- $m = 30$ is used as the dimension of the Krylov subspace for the restarted GMRES method.

As shown in Figure 2(a), the first example is a $3.375\,\mathrm{m} \times 3.375\,\mathrm{m}$ PEC plate buried in a lossy ground with $\varepsilon_{r1} = 4$, $\mu_{r1} = 4$, and $\sigma_1 = 0.01\,\mathrm{S/m}$, $0.5\,\mathrm{m}$ below the free-space-ground interface. The plate is discretized with 10462 triangular patches leading to 15557 unknowns. The second example is a perfectly electrically conducting (PEC) cylinder situated over a half space as shown in Figure 3(a). The cylinder is 3 m long, has a diameter of 1 m, and is situated 20 cm above Yuma soil of 10% water content characterized by $\varepsilon_{\mathrm{half}} = 6 - j0.5$ and $\mu_{\mathrm{half}} = 1.0$. The cylinder is discretized with 10092 triangular patches leading to 15138 unknowns. The last example is PEC rectangular box with size $L_x \times L_y \times L_z = 12 \times 2 \times 2.5\,\mathrm{m}^3$ situated 50 cm above Yuma soil

with 10% water content characterized by $\varepsilon_{\text{half}} = 6 - j0.5$ and $\mu_{\text{half}} = 1.0$ in Figure 4(a). The cylinder is discretized with 6564 triangular patches leading to 9846 unknowns. Figure 2(b) shows the bistatic RCS for $\theta_{\text{scat}} = 45°$ for the first example. The incident angles of plane wave are $\theta_{\text{inc}} = 0°$ and $\phi_{\text{inc}} = 0°$ at a frequency of $f = 300\,\text{MHz}$. MLFMA with 3 levels is used to accelerate the matrix-vector products. It can be found that the results using the MLFMA are in good agreement with that of the MoM analysis [29]. Figure 3(b) shows the co-polarized (VV and HH) and cross-polarized (VH and HV) bistatic RCS for $\theta_{\text{scat}} = 60°$ for the second cylinder example at 600 MHz. The incident angles of plane wave are $\theta_{\text{inc}} = 60°$ and $\phi_{\text{inc}} = 0°$. The bistatic RCS for $\theta_{\text{scat}} = 80°$ for the third rectangular box example is given in Figure 4(b). The incident angles of plane wave are $\theta_{\text{inc}} = 60°$ and $\phi_{\text{inc}} = 60°$ at 150 MHz.
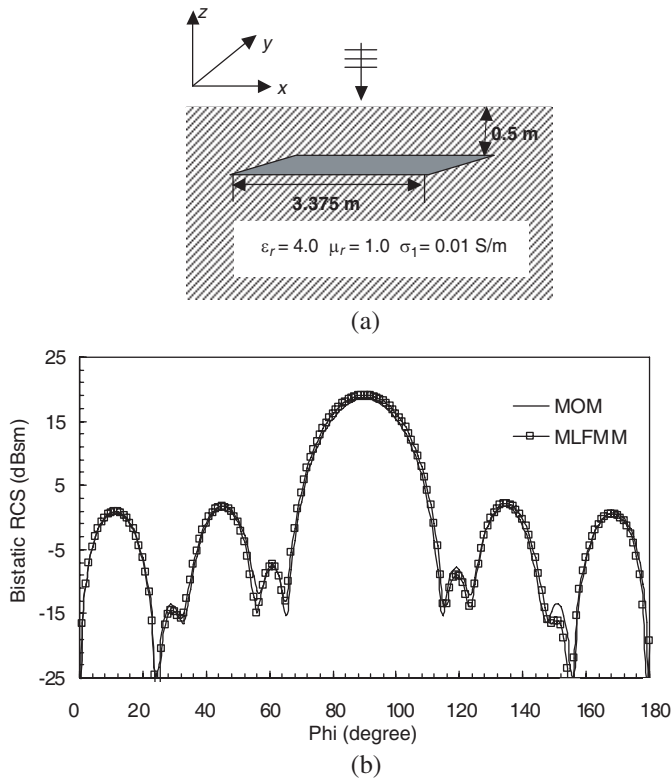

(a)

(b)

Figure 2. (a) Geometry of a PEC plate buried in a lossy ground. (b) The bistatic RCS of plate buried in lossy ground for $\theta_{\text{scat}} = 45°$ at 300 MHz.
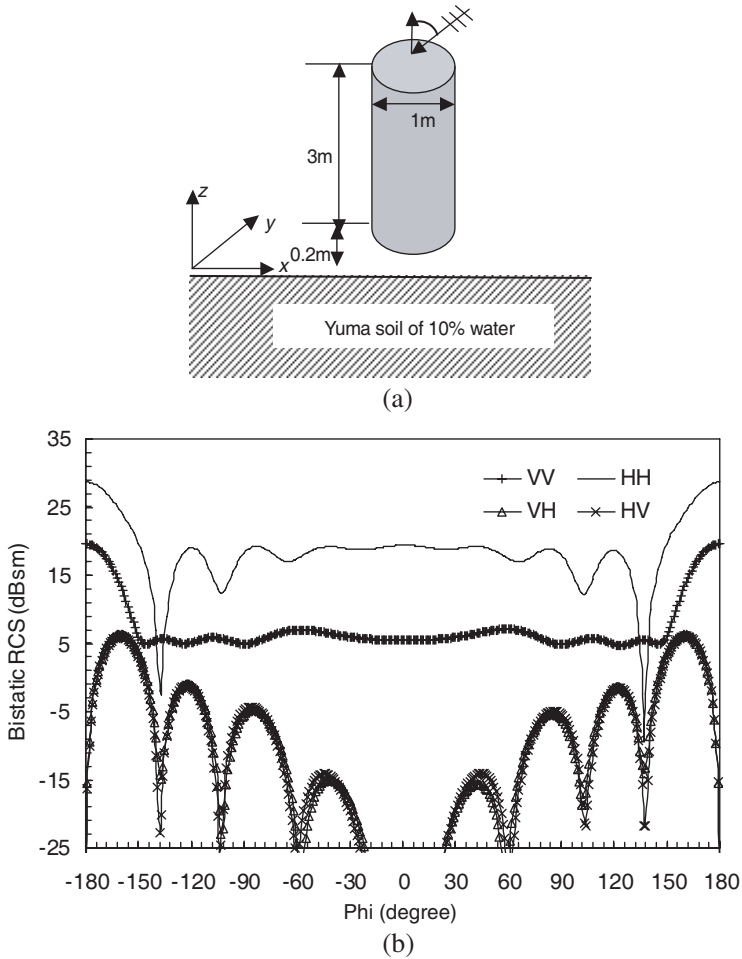
(a)

(b)

Figure 3. (a) Geometry of a conducting cylinder situated $20\,\mathrm{cm}$ above Yuma soil of 10% water. (b) The bistatic RCS of a conducting cylinder situated $20\,\mathrm{cm}$ above Yuma soil of 10% water content for $\theta_{\mathrm{scat}} = 60°$ at $600\,\mathrm{MHz}$.

MLFMA with 2 levels is used in RCS calculation for the last two examples. From Figures 2, 3, the MLFMA results agree well with the results in [1, 30].

Next, we investigate the performance of the two-step spectral preconditioner on electromagnetic scattering of the above three examples. Figures 5–7 show the convergence history of GMRES algorithms with different preconditioners for all examples, where Diag

denotes the diagonal preconditioner; ILU0 denotes the incomplete LU decomposition preconditioner with no fill-ins during the construction process [25]; SSOR denotes the symmetric successive over-relaxation preconditioner; MSAI denotes the improved SAI preconditioner based on MLFMA implementation [19]; Two-step stands for the the two-step spectral preconditioner suggested in this paper. In these computations, 10 approximate smallest eigenvectors ($k = 10$), extracted by GMRES-
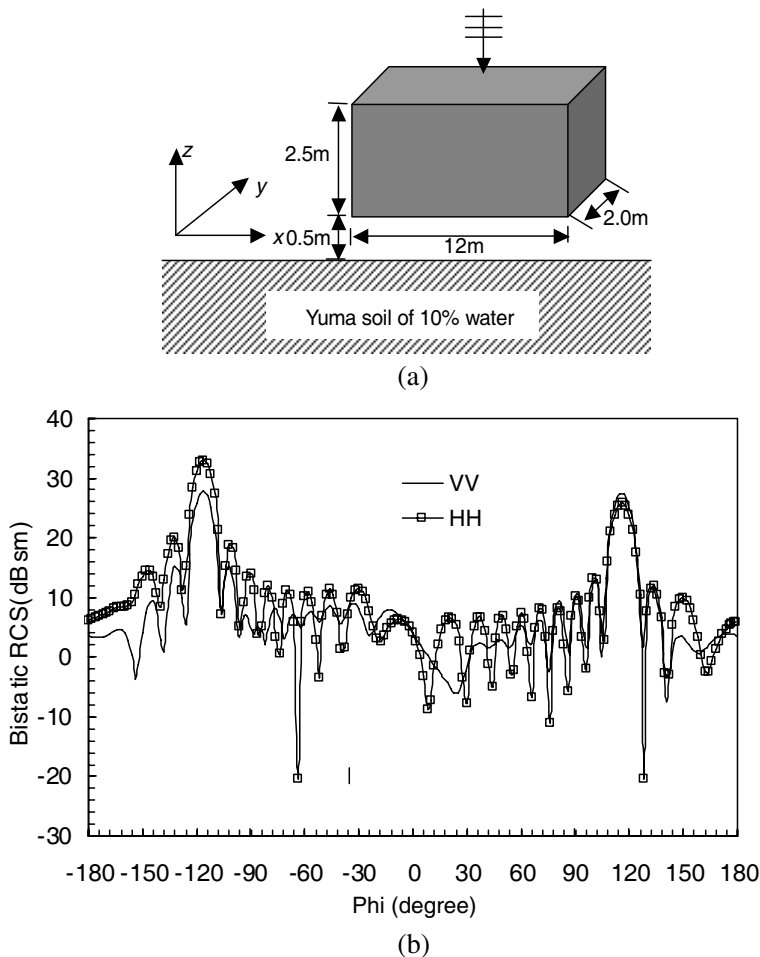

(a)

(b)

Figure 4. (a) Geometry of a closed rectangular box situated 50 cm above Yuma soil of 10% water content. (b) The co-polarized bistatic RCS (VV and HH) of a closed rectangular box situated 50 cm above Yuma soil of 10% water content for $\theta_{\text{scat}} = 80°$ at 150 MHz.

DR algorithm during solving EFIE system, are employed to build the two-level spectral preconditioner M_2 for the three examples. 1.0 is taken as the relaxation parameter for building the SSOR preconditioner. It can be found that GMRES algorithm with none, Diag, ILU0, SSOR preconditioner can not converge in 1000 iterations for the half-space cylinder and rectangular box examples in Figures 6, 7. We found that both the MSAI and proposed two-step spectral preconditioned GMRES methods converge faster than the other preconditioning techniques for the above three half-space examples. When compared with MSAI preconditioned GMRES, the two-step spectral preconditioned GMRES decreases the number of iterations by a factor of 5.2 on the Plate example buried in lossy ground, 4.1 on the half-space cylinder example. Furthermore, it can be observed that the MSAI preconditioned GMRES cannot converge in 1000 iterations while the proposed two-step spectral preconditioned GMRES converges in less than 150 iterations for the rectangular box examples in Figure 7. This demonstrates the efficiency of the newly proposed two-step spectral preconditioner for the half-space scattering problems.

Since a good preconditioner depends not only on its effect on convergence but also on its construction and implementation time. Tables 1–3 list the construction time and total solution time of GMRES algorithms with different preconditioners on the above three examples, where * refers to no convergence after maximum 1000 iterations,
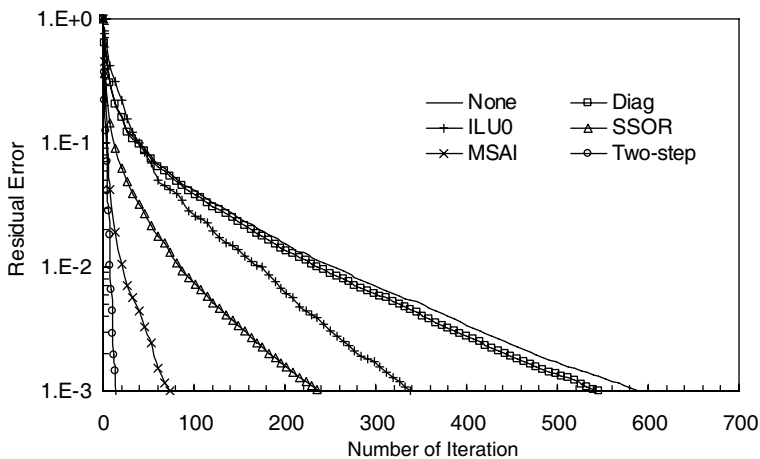

Figure 5. Convergence history of GMRES algorithms on the plate example buried in lossy ground.
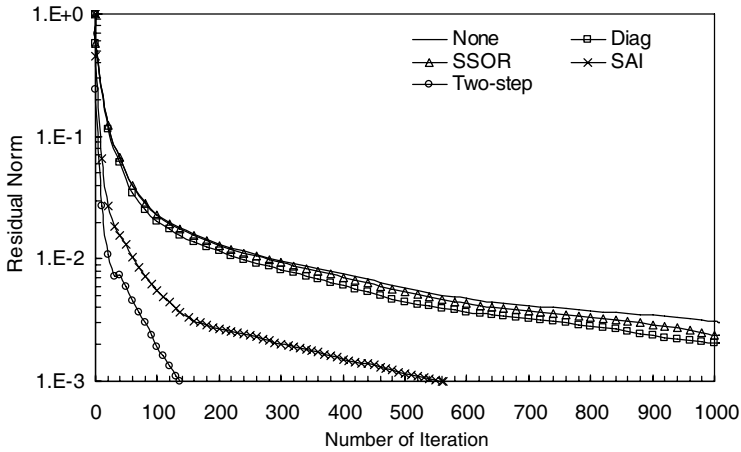
Figure 6. Convergence history of GMRES algorithms on a conducting cylinder situated 20 cm above Yuma soil of 10% water content.
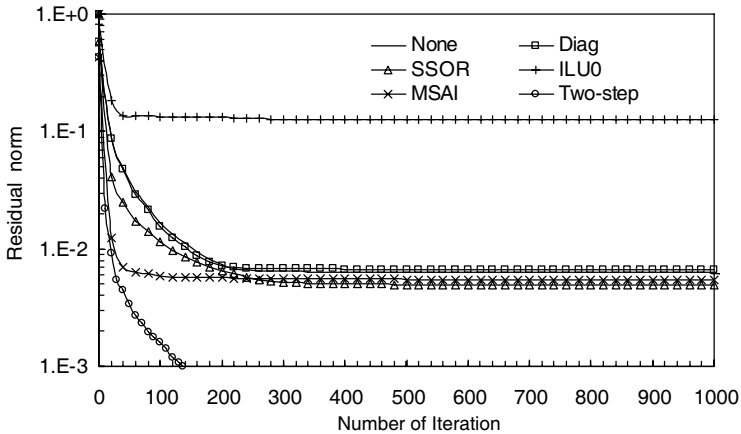

Figure 7. Convergence history of GMRES algorithms on a rectangular box situated 50 cm above Yuma soil of 10% water content.

and the density of a preconditioner is defined by the ratio of the number of non-zero entries in the preconditioning matrix to the number of entries in the full EFIE impedance matrix. In our numerical experiments, the convergence of ILU0 preconditioned GMRES is very unstable for the conducting cylinder example in Table 2. Though the ILU0 preconditioned GMRES converges in less than 5 iteration steps for this example, the bistatic RCS is incorrect in the numerical

Table 1. Comparison of the cost and performance of different preconditioners on the Plate example buried in lossy ground.

	Density	Construction time	Iterations	Solution time	Total time
None	-	-	590	307 s	307 s
Diag	-	-	546	608 s	608 s
SSOR	1.21%	-	239	307 s	307 s
ILU0	1.21%	20 s	338	460 s	480 s
MSAI	2.77%	967 s	72	102 s	1069 s
Two-step	2.77%	1056 s	14	21 s	1077 s

Table 2. Comparison of the cost and performance of different preconditioners on a conducting cylinder situated 20 cm above Yuma soil of 10% water content.

	Density	Construction time	Iterations	Solution time	Total time
None	-	-	3941	4593 s	4593 s
Diag	-	-	1780	3537 s	3537 s
SSOR	1.47%	-	1986	4627 s	4627 s
MSAI	0.81%	71 s	563	800 s	871 s
Two-step	0.81%	130 s	137	245 s	375 s

experiment. Therefore, the numerical results for ILU0 are meaningless for the half-space conducting cylinder example, and they are omitted in Table 2. From Tables 1–3, it can be found that the proposed spectral preconditioned GMRES method can reduce the number of iterations significantly while the constructing time of the preconditioner is more than the other preconditioning methods. Compared with the MSAI preconditioner, the additional construct time of the two-step spectral preconditioner is only the construct time of the spectral preconditioner M_2 obtained from GMRES-DR algorithm after solving EFIE system. From Table 1 for the first example, we found that the total solution time (including both the construction time and the iterative solution time) of the two-step spectral preconditioned GMRES is more than the

Table 3. Comparison of the cost and performance of different preconditioners on a rectangular box situated 50 cm above Yuma soil of 10% water content.

	Density	Construction time	Iterations	Solution time	Total time
None	-	-	*	*	*
Diag	-	-	*	*	*
SSOR	1.85%	-	*	*	*
ILU0	1.85 %	12 s	*	*	*
MSAI	1.40%	49 s	*	*	*
Two-step	1.40%	381 s	136	164 s	545 s

other preconditioned methods though the solution time of the proposed method is less than the other methods. For the other two examples in Tables 2–3, it can be found that the two-step spectral preconditioned GMRES can save much time than other methods.

All the numerical experiments reported so far have been obtained for the fixed size of the spectral preconditioner with $k = 10$ for the three examples. A critical question in the use of the two-step spectral preconditioned GMRES algorithm is how to choose the number k of approximately smallest eigenvectors. In the following, the effect of the size of the spectral preconditioner is investigated on the efficiency of the two-step spectral preconditioner. For each value k of the spectral preconditioner, the number of GMRES iterations of the two-step spectral preconditioned GMRES algorithm is shown in Table 4, where * refers to that the number of GMRES iterations is more than the maximum 1000 iterations. Example 1 denotes the above Plate example buried in lossy ground; Example 2 denotes the above half-space conducting cylinder example; Example 3 denotes the above half-space rectangular box example. The number of iteration corresponding to $k = 0$ is just the number of iteration for the MSAI preconditioned GMRES algorithm. Generally speaking, if the larger size of the spectral preconditioner is chosen, the better of the two-level preconditioner is to be expected. In practice, however, it is not the case. Firstly, there is no easy way to compute eigenvector information inexpensively and accurately. In this paper, the smallest eigenvectors are approximately computed as a byproduct of GMRES-DR algorithm during solving the EFIE system.

Table 4. Sensitivity of the two-step spectral preconditioner with respect to the size k of the spectral preconditioner.

		Size of the spectral preconditioner k							
Geometry	Density	0	8	10	15	18	20	25	30
Example 1	2.77%	73	14	13	15	14	13	13	13
Example 2	0.81%	563	128	128	128	131	131	137	128
Example 3	1.40%	*	136	136	134	137	132	134	132

The roughly approximated smallest eigenvectors usually have little influence on the performance of the spectral preconditioner. Secondly, it is difficult to compute those smallest eigenvectors, which are very close to each other. Therefore, approximations to some of smallest eigenvectors maybe not significantly help convergence.

5. CONCLUSION

In this paper, the two-step spectral preconditioning technique is presented for solving EFIE for scattering from conducting objects above or buried in a lossy half-space. Half-space MLFMA is used to reduce computational complexity. The combined effect of the SAI preconditioner that damps the high frequencies of the iteration error, coupled with the spectral preconditioner that eliminates the low frequencies is very beneficial for the convergence of GMRES. Numerical experiments are performed and the comparison is made with the other preconditioners. It can be found that the proposed two-step spectral preconditioning technique is more efficient and can significantly reduce the overall computational cost.

For solving large-scale electromagnetic problem, effective parallelization of both matrix-vector products and iterative solvers should be considered. Recent attempts have yielded efficient parallelization of the MLFMA. Constructing parallel and efficient preconditioners is currently an important bottleneck for the solution of large electromagnetic problems. For constructing the parallel two-step spectral preconditioner, parallel SAI preconditioning matrix $\mathbf{M}_1$ should be firstly constructed based on the sparse near-field matrix in MLFMA. Then,

the parallel SAI preconditioned GMRES-DR algorithm should be constructed to obtained the spectral preconditioning matrix $\mathbf{M}_2$. For constructing the parallel GMRES-DR algorithm, the greatest challenge is the parallelization of deflating with eigenvectors removed from Krylov subspace. Further investigations deserve to be undertaken to study parallelization of the proposed spectral preconditioner for large-scale electromagnetic calculation.

ACKNOWLEDGMENT

REFERENCES

1. Geng, N., A. Sullivan, and L. Carin, "Multilevel fastmultipole algorithm for scattering from conducting targets above or embedded in a lossy half space," *IEEE Trans. Geosci. Remote Sensing*, Vol. 38, No. 4, 1561–1573, Jul. 2000.

2. Liu, Z. J., J. Q. He, Y. J. Xie, A. Sullivan, and L. Carin, "Multilevel fast multipole algorithm for general targets on a half-space interface," *IEEE Trans. Antennas Propagat.*, Vol. 50, No. 12, 1838–1849, Dec. 2002.

3. Li, L., J. Q. He, Z. J. Liu, X. L. Dong, and L. Carin, "MLFMA analysis of scattering from multiple targets in the presence of a half-space," *IEEE Trans. Antennas Propagat.*, Vol. 51, No. 4, 810–819, Apr. 2003.

4. Geng, N., A. Sullivan, and L. Carin, "Fast multipole method for scatering from an arbitrary PEC target above or buried in a lossy half space," *IEEE Trans. Antennas Propagat.*, Vol. 49, No. 5, 740–748, May 2001.

5. Harrington, R. F., *Field Computation by Moment Methods*, R. E. Krieger, Malabar, Fla., 1968.

6. Rao, S. M., D. R. Wilton, and A. W. Glisson, "Electromagnetic scattering by surfaces of arbitrary shape," *IEEE Trans. Antennas Propagat.*, Vol. 30, No. 3, 409–418, 1982.

7. Chew, W. C., J. M. Jin, E. Midielssen, and J. M. Song, *Fast and*

Efficient Algorithms in Computational Electromagnetics, Artech House, Boston, MA, 2001.

8. Shubair, R. M. and Y. L. Chow, "A simle and accurate complex image interpretation of vertical antennas present in contiguous dielectric halfspaces," *IEEE Trans. Antennas Propagat.*, Vol. 41, 806–812, Jun. 1993.

9. Aksun, M. I., "A robust approach for the derivation of closed-form Green's functions," *IEEE Trans. Microw. Theory Tech.*, Vol. 44, 651–658, May 1996.

10. Geng, N., A. Sullivan, and L. Carin, "Fast multipole method for scattering from 3D PEC targets situated in a half-space environment," *Microwave and Optical Technology Letters*, Vol. 21, 399–405, Jun. 1999.

11. Chew, W. C., I. T. Chiang, et al., "Integral equation solvers for real world applications — Some challenge problems," *Proceedings of IEEE International Symposium on Antennas and Propagat.*, 91–93, Albuquerque, NM, 2006.

12. Song, J. M., C. C. Lu, and W. C. Chew, "Multilevel fast multipole algorithm for electromagnetic scattering by large complex objects," *IEEE Trans. Antennas Propagat.*, Vol. 45, No. 10, 1488–1493, Oct. 1997.

13. Sertel, K. and J. L. Volakis, "Incomplete LU preconditioner for FMM implementation," *Microwave and Optical Technology Letters*, Vol. 26, No. 7, 265–267, 2000.

14. Chow, E. and Y. Saad, "Experimental study of ILU preconditioners for indefinite matrices," *Journal of Computational and Applied Mathematics*, Vol. 86, 387–414, 1997.

15. Carpentieri, B., I. S. Duff, L. Griud, and G. Alleon, "Combining fast multipole techniques and an approximate inverse preconditioner for large electromagnetism calculations," *SIAM Journal on Scientific Computing*, Vol. 27, No. 3, 774–792, 2005.

16. Malas, T. and L. Gurel, "Accelerating the multilevel fast multipole algorithm with the sparse-approximate-inverse (SAI)," *SIAM Journal on Scientific Computing*, Vol. 31, No. 3, 1968–1984, 2009.

17. Andriulli, F. P., K. Cools, H. Bagci, F. Olyslager, A. Buffa, S. Christiansen, and E. Michielssen, "A Multiplicative calderon preconditioner for the electric field integral equation," *IEEE Trans. Antenna Propagat.*, Vol. 56, No. 8, 2398–2412, August 2008.

18. Carpentieri, B., I. S. Duff, and L. Griud, "Sparse pattern selection strategies for robust frobenius-norm minimization preconditioners

in electromagnetism," *Numerical Linear Algebra Applications*, Vol. 7–8, No. 7–8, 667–685, 2000.

19. Ding, D.-Z., R. S. Chen, and Z. H. Fan, "An efficient sai preconditioning technique for higher order hierarchical MLFMM implementation," *Progress In Electromagnetics Research*, PIER 88, 255–273, 2008.

20. Erhel, J., K. Burrage, and B. Pohl, "Restarted GMRES preconditioned by deflation," *Journal of Computational and Applied Mathematics*, Vol. 69, 303–318, 1996.

21. Rui, P. L., R. S. Chen, D. X. Wang, and E. K. N. Yung, "Spectral two-step preconditioning of multilevel fast multipole algorithm for the fast monostatic RCS calculation," *IEEE Trans. Antennas Propagat.*, Vol. 55, No. 8, August 2007.

22. Ding, D. Z., R. S. Chen, Z. H. Fan, and P. L. Rui, "A novel hierarchical two-level spectral preconditioning technique for multilevel fast multipole analysis of electromagnetic wave scattering," *IEEE Trans. Antennas Propagat.*, Vol. 56, No. 4, 1122–1132, April 2008.

23. Michalski, K. A. and D. Zheng, "Electromagnetic scattering and radiation by surfaces of arbitrary shape in layered media, Parts I and II," *IEEE Trans. Antennas Propagat.*, Vol. 38, 335–352, Mar. 1990.

24. Lindell, I. V., *Methods for Electromagnetic Field Analysis*, IEEE Press, Piscataway, NJ, 1995.

25. Saad, Y., *Iterative Methods for Sparse Linear Systems*, PWS Publishing Company, 1996.

26. Van Der Vorst, H. A. and C. Vuik, "The superlinear convergence behaviour of GMRES," *Journal of Computational and Applied Mathematics*, Vol. 48, 327–341, 1993.

27. Lehoucq, R. B., D. C. Sorensen, and C. Yang, "ARPACK User's guide: Solution of large-scale problem with implicitly restarted Arnoldi methods," *SIAM*, Philadelphia, 1998.

28. Morgan, R. B, "GMRES with deflated restarting," *SIAM Journal of Scientific Computing*, Vol. 24, 20–37, 2002.

29. Bağcı, H., A. E. Yılmaz, V. Lomakin, and E. Michielssen, "Fast solution of mixed-potential time-domain integral equations for half-space environments," *IEEE Trans. Geosci. Remote Sensing*, Vol. 43, No. 2, 269–279, May 2005.

30. Geng, N. and L. Carin, "Fast multipole method for targets above or buried in lossy soil," *IEEE Antennas and Propagat. Society International Symposium*, 644–647, 1999.